Speed of Sound Measurements Using a Cylindrical Resonator for Gaseous Carbon Dioxide and Propene

ARTICLE *in* JOURNAL OF CHEMICAL & ENGINEERING DATA · SEPTEMBER 2014

Impact Factor: 2.04 · DOI: 10.1021/je500424b

4 AUTHORS, INCLUDING:

Qiang Liu
Tsinghua University
13 PUBLICATIONS **65** CITATIONS
SEE PROFILE

Xiaojuan Feng
National Institute of Metrology
19 PUBLICATIONS **97** CITATIONS
SEE PROFILE

Journal of chemical & engineering data

Article

pubs.acs.org/jced

Speed of Sound Measurements Using a Cylindrical Resonator for Gaseous Carbon Dioxide and Propene

Qiang Liu,[†,‡] Xiaojuan Feng,[§] Baolin An,[†] and Yuanyuan Duan*[,†]

[†]Key Laboratory of Thermal Science and Power Engineering of MOE, Beijing Key Laboratory for CO_2 Utilization and Reduction Technology, Tsinghua University, Beijing 100084, China

[‡]College of Mechanical and Transportation Engineering, China University of Petroleum, Beijing 102249, China

[§]Division of Thermophysics and Process Measurements, National Institute of Metrology, Beijing 100013, China

ABSTRACT: Carbon dioxide (R744) and propene (R1270) are expected to be long-term working fluids for air conditioning systems, heat pumps, and organic Rankine cycles (ORCs) because of their low global warming potentials (GWP). The speed of sound was measured in gaseous carbon dioxide from (260 to 333) K and in gaseous propene from (260 to 330) K using a cylindrical resonator at pressures up to 1 MPa. The perturbations from the thermal and viscous boundary layers, the gas fill duct, the shell motion, and the vibrational relaxation were corrected in the frequency measurements. The uncertainties in the temperature, pressure, and speed of sound measurements were estimated to be less than 5 mK, 200 Pa, and 0.02 %. The ideal-gas heat capacities at constant pressure and the acoustic virial coefficients of carbon dioxide and propene were deduced from the measured speed-of-sound data. The second virial coefficients for carbon dioxide and propene were obtained from the acoustic data and the square-well intermolecular model.

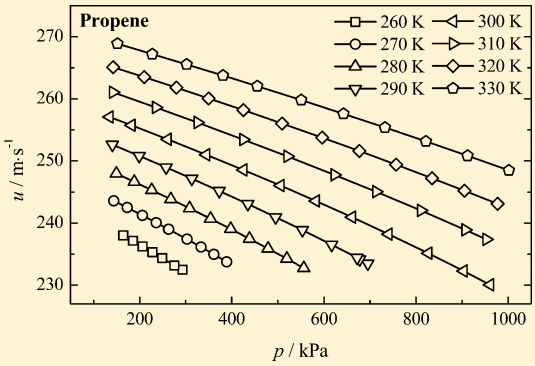

1. INTRODUCTION

HCFC and HFC emissions from air conditioning, refrigeration, chiller, and heat pump systems contribute significantly to global warming. Environment friendly and energy efficient refrigerants are the main route to reduce the greenhouse gas emissions. Carbon dioxide (R744) has good environmental properties such as being nonflammable, nontoxic, nonozone depleting, and having negligible global warming potential (GWP). Carbon dioxide is also cheap and widely available. Recent studies have indicated that carbon dioxide can be used to replace chlorodifluoromethane (R22) or 1,1,1,2-tetrafluoroethane (R134a) in air conditioning applications, heat pumps, and chillers.[1−4] Propene (R1270) has similar thermophysical properties with R22 such as normal boiling point, saturation pressure, and critical temperature, but the GWP of propene is much lower. Therefore, propene is expected to be an R22 alternative in air conditioning and heat pump systems.[5−9] Propene has also been studied as an alternative to R502 in low temperature refrigeration applications.[10]

The organic Rankine cycle (ORC) is the preferred technique to convert medium-low temperature thermal energy to electricity. One of the critical challenges with ORCs is the working fluid selection.[11−15] Some environmentally friendly fluids can be used as working fluids for ORC systems,[16,17] and carbon dioxide[18−21] and propene[11,12,20,22,23] have been considered as working fluids for ORC systems driven by low-grade heat sources.

Accurate thermodynamic properties are the needed for system design and optimization.[24] The speed of sound is an important thermophysical property that can be accurately measured. The ideal-gas heat capacity, the virial coefficients and the isentropic compressibility can then be determined from the speed-of-sound data.[25−34] The isobaric heat capacity and the compression factor are linked to the speed of sound based on rigorous thermodynamic theory and can be determined using numerical integration of the differential equations.[26,33−36]

Acoustic resonators have been the preferred method for measuring the speed of sound and various thermodynamic properties,[25−48] the Boltzmann constant, k_B,[49−54] and thermodynamic temperatures.[55−60] Spherical resonators have been widely used because of their high quality factors and high measurement precision. Cylindrical resonators have lower quality factors, but they are easier to manufacture and assemble. The experimental system and correction methods for perturbations due to imperfections on the resonant frequency measurement have been significantly improved in recent years.[41,42,53,61−64] The relative standard uncertainty in the Boltzmann constant, k_B, can reach 3.7×10^{-6} using a fixed-length cylindrical resonator.[54] This paper presents speed of sound measurements using a cylindrical resonator for gaseous carbon dioxide and propene.

Received: May 12, 2014
Accepted: August 4, 2014
Published: August 13, 2014

dx.doi.org/10.1021/je500424b | J. Chem. Eng. Data 2014, 59, 2788−2798

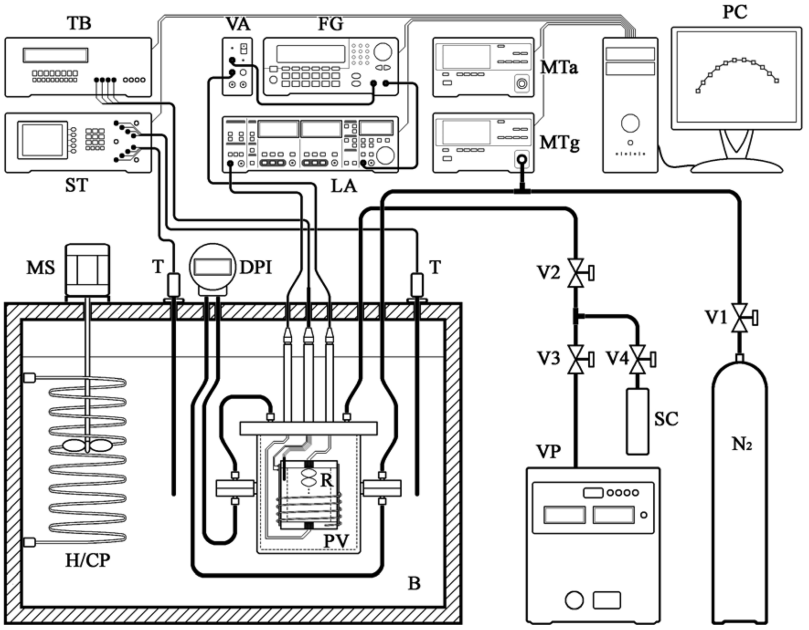

Figure 1. Schematic diagram of the experimental system for the speed of sound measurements: B, thermostatic bath; DPI, differential pressure transducer; FG, function generator; H/CP, heater/cooler; LA, lock-in amplifier; MS, mechanical stirrer; MTa, absolute pressure digital manometer; MTg, gauge pressure digital manometer; PC, personal computer; PV, pressure vessel; R, resonator; SC, sample cylinder; ST, super thermometer; T, platinum resistance thermometer; TB, thermometer bridge; VA, voltage amplifier; VP, vacuum pump; V1 to V4, valves.

2. EXPERIMENTAL SECTION

Measurement Fundamentals. For a geometrically perfect and rigid cylindrical resonator with radius, a, and length, L, the unperturbed resonant frequency, f^0_{lmn}, of mode (lmn) is given by[26,34,41]

$$f^0_{lmn} = \frac{u}{2\pi}\sqrt{\left(\frac{l\pi}{L}\right)^2 + \left(\frac{\chi_{m,n}}{a}\right)^2} \quad (1)$$

where u is the speed of sound, the positive integer l is the order of the longitudinal mode, and $\chi_{m,n}$ is a root of $dJ_m(x)/dx = 0$ in which $J_m(x)$ is the mth order Bessel function.

For longitudinal modes $\chi_{m,n} = 0$; therefore, the speed of sound, u, can be determined using longitudinal modes $(l00)$ by

$$u = \frac{2L}{l} f^0_{l00} \quad (2)$$

where f^0_{l00} denotes the unperturbed resonant frequencies of the longitudinal modes $(l00)$.

Accurate resonant frequency measurements are the basis for determining the speed of sound. However, the gas-shell boundary of the cylindrical resonator has nonzero thermal and viscous admittances that cause the measured resonant frequencies to differ from their unperturbed values. The geometry of a practical resonator is also not perfect. A gas fill duct used to admit the gas into and out of the resonator is an opening in the resonator wall which disturbs the resonant frequency. The shell and the end plates of practical cylindrical resonators are also not rigid, thus the resonator shell deforms due to the shell motion during the measurements and the mechanical admittance associated with the shell deformations disturbs the frequency and enlarges the half-width of the signal peak.[53,61] In addition, the lead zirconate titanate (PZT) source transducer is bonded to the outer surface of the flexible, thin diaphragm in the resonator end plates, and the deformation and motion of the transducer affects the resonate frequency. The vibrational relaxation times of some polyatomic gases such as carbon dioxide are sufficiently long for the measured frequency range to overlap with the region of significant dispersion. Therefore, the unperturbed resonant frequency, f^0_{l00}, must be related to the measured frequency, f_N, as

$$f^0_{l00} = f_N - \Delta f_{th} - \Delta f_v - \Delta f_{sh} - \Delta f_d - \Delta f_{tr} - \Delta f_{vib} \quad (3)$$

where f_N is the measured resonant frequency, Δf_{th} is the frequency perturbation from the thermal boundary layer, Δf_v is the frequency perturbation from the viscous boundary layer, Δf_{sh} is the frequency perturbation from the shell motion, Δf_d is the frequency perturbation from the gas fill duct, Δf_{tr} is the frequency perturbation from the transducers, and Δf_{vib} is the frequency perturbation from the vibrational relaxation.

The perturbations from the thermal and viscous boundary layers, the gas fill duct, the shell motion and the vibrational relaxation on the resonant frequency measurement using a cylindrical resonator have been thoroughly discussed elsewhere.[26,34,41,46,53,54,61−63] Here, Δf_{th}, Δf_v, and Δf_{sh} were calculated using the models from Zhang et al.,[53,61] Δf_d was calculated using the model developed by Gillis et al.,[62] Δf_{tr} was calculated using the model developed by Lin et al.[63] and Δf_{vib} was calculated using the method described by Estrada-Alexanders and Trusler[44] and Hurrly.[46]

Apparatus. A diagram of the apparatus used for the speed of sound measurements is shown in Figure 1.[64] The system consisted of a cylindrical resonator, a frequency measurement system, thermostatic baths, a temperature measurement system, a pressure measurement system, a vacuum system, and a data acquisition system.

The cylindrical resonator was made of stainless steel (316 SS) with an inner length of 80.7 mm and a radius of 40 mm. The resonator was hung in a pressure vessel with a flexible connector. Many efforts were made to improve the signal-to-noise ratio because the quality factor, Q, for a cylindrical

dx.doi.org/10.1021/je500424b | J. Chem. Eng. Data 2014, 59, 2788−2798

resonator is lower than that in a spherical resonator. Piezoelectric ceramics were used as the source and detector transducers to increase the acoustic response. A gas-filled duct was arranged in the middle of the resonator for the gas inlet and outlet.

The cylindrical resonator length and radius were determined from acoustic measurements in gaseous argon from (270 to 333.15) K and pressures from (60 to 1010) kPa. The argon was provided by Beiwen Gas Corp. with a stated mole purity of 99.999 %. The measured resonant frequency was corrected based on eq 3 with the densities, specific heat capacities, and the specific heat ratio calculated by the equation of state developed by Tegeler et al.[65] and the viscosities and thermal conductivities calculated using the equation given by Lemmon and Jacobsen.[66]

The drive voltage to the PZT source transducer was generated by a function generator (model Agilent 33220A) and amplified by a voltage amplifier (model GRAS 14AA). A lock-in amplifier (model SRS 830) with a reference frequency from the function generator was used to measure the acoustic response of the PZT detector. The resonant frequency was then fit by the personal computer according to signals from the lock-in amplifier. The uncertainty in the frequency measurement was estimated to be $5 \times 10^{-6} f^0$.

A capsule platinum resistance thermometer (model HART 5686) enclosed in the cylindrical resonator wall and a superthermometer (model HART 1590) were used to measure the gas temperature in the resonator. The thermostatic bath fluid temperature was measured by a standard platinum resistance thermometer (model Tinsley 5187SA). The overall temperature uncertainty was estimated to be within 5 mK, including the 2 mK uncertainty of the capsule platinum resistance thermometer, the 1 mK uncertainty of the superthermometer, and the 3 mK stability and uniformity uncertainty of the resonator. The temperature was determined on the basis of the International Temperature Scale of 1990 (ITS-90). Before the experiments, the platinum resistance thermometers, the superthermometer, and the digital manometers were calibrated by the National Institute of Metrology (NIM), China.

An absolute digital manometer (model Yokogawa, MT 210, 0 kPa to 130 kPa), a gauge pressure digital manometer (model Yokogawa, MT 210, 0 kPa to 3500 kPa), and a sensitive diaphragm pressure transducer (model Rosemount 3051S, 2 kPa to 20 kPa) were used to control and measure the gas pressure in the resonator. The pressure uncertainty was estimated to be less than 200 Pa including the uncertainty of the absolute digital manometer of 30 Pa from (0 to 130) kPa, the uncertainty of the gauge pressure digital manometer of 80 Pa from (0 to 3500) kPa and the uncertainty of the differential pressure detector of less than 20 Pa.

A turbo-molecular pump (model KYKY, FD 110) with an extreme vacuum of $1 \cdot 10^{-6}$ Pa was used to evacuate the experimental system and the sample cylinder.

A gas chromatograph (model Shimadzu, GC 2014) with a thermal conductivity detector and a 3 m × 3 mm Porapak-Q column was used to measure the sample purity. Helium (99.999 %) was used as the carrier gas at a flow rate of 45 $cm^3 \cdot min^{-1}$. The oven and TCD temperatures were set to 373 K. After injection of the sample into the column, the effluence was analyzed for 15 min.

Experimental Procedures. The speed of sound was measured at pressures below 1000 kPa. The highest pressure was less than 80 % of the saturation pressure for propene from (260 to 290) K to prevent precondensation.[67] Part of the sample was then discharged to reach a lower pressure after the measurements at one pressure were completed. The discharged samples were collected in an evacuated cylinder and then introduced into the GC system to check the gas purity.

The resonant frequencies, f_N, and half-widths, g_N, of several acoustic modes were measured precisely using the following procedure. First, f_N and g_N were estimated from either a preliminary measurement or a theoretical calculation. Then, the signal from the detector was measured at 11 drive frequencies from $f_N - g_N$ to $f_N + g_N$ increasing in increments of $g_N/5$, followed by the frequency sweep being reversed from $f_N + g_N$ to $f_N - g_N$. Performing the frequency sweep in both directions reduces the impacts of small temperature and pressure drifts on the resonant frequency. The dwell time at each frequency was 5 s. The temperature and pressure of the sample were measured simultaneously at each drive frequency. The 22 frequencies and the in-phase voltages, U, and the quadrature voltages, V, were then fit to

$$U + iV = \frac{if\mathbf{A}}{f^2 - \mathbf{F}_N^2} + \mathbf{B} + \mathbf{C}(f - \tilde{f}) \quad (4)$$

where **A**, **B**, and **C** are complex constants and $\mathbf{F}_N = f_N + ig_N$ is the complex resonant frequency of the mode under study. The parameters **B** and **C** take into account possible crosstalk and the effects of the "tails" of modes other than the one under study.

Samples. The CO_2 sample was obtained from Beiwen Gas Corp. with a stated mole purity of 99.995 %, and the propene sample was obtained from Kedi Gas Corp. with a stated mole purity of 99.95 % (see Table 1). The samples were used without further purification except for being cooled in liquid nitrogen and evacuated by a vacuum pump to remove possible air impurities. The sample before filling the resonator and the collected samples that were discharged to reduce the experimental pressures were analyzed by the GC system. The impurities in the CO_2 were measured to be less than 0.005 % and in the propene to be less than 0.03 %.

Table 1. Chemical Sample Description

chemical name	source	initial purity	purification method	final purity	analysis method
carbon dioxide	Beiwen Gas Corp.	99.995 %	none	99.995 %	GC[a]
propene	Kedi Gas Corp.	99.95 %	degassing	99.97 %	GC

[a]Gas chromatography.

3. RESULTS AND DISCUSSION

3.1. Speed of Sound. The measured speed-of-sound data in gaseous carbon dioxide along nine isotherms from (260 to 332.75) K with pressures up to 1000 kPa are listed in Table 2. The relative standard uncertainty of the speed of sound for gaseous carbon dioxide was estimated to be less than 0.02 % including the temperature measurement uncertainty, the pressure measurement uncertainty, the frequency measurement uncertainty, and the sample purity uncertainty. The relative deviations of the measured speed of sound in gaseous carbon dioxide from the equation of state developed by Span and

Table 2. Measured Speed of Sound Data for Gaseous Carbon Dioxide[a]

p/kPa	u/m·s^{-1}	p/kPa	u/m·s^{-1}
	T = 260.000 K		
884.92	242.761	562.69	246.845
822.03	243.577	501.31	247.598
760.19	244.370	434.17	248.411
701.21	245.119	379.95	249.058
626.77	246.054	317.37	249.804
	T = 270.000 K		
977.38	247.218	556.68	251.923
906.73	248.028	460.73	252.960
819.89	249.014	362.27	254.006
732.10	249.996	305.05	254.606
644.89	250.959		
	T = 280.000 K		
981.82	252.563	537.04	256.947
884.20	253.546	453.25	257.750
798.98	254.394	362.38	258.608
692.20	255.443	280.31	259.377
621.46	256.133		
	T = 290.000 K		
819.49	259.125	421.86	262.559
733.65	259.876	355.64	263.124
655.16	260.559	282.86	263.732
571.60	261.280	228.71	264.190
490.56	261.978		
	T = 300.000 K		
1017.33	262.360	583.49	265.756
927.15	263.073	500.85	266.392
847.25	263.703	415.37	267.046
755.49	264.422	340.26	267.619
663.90	265.134	280.85	268.065
	T = 304.090 K		
968.58	264.694	544.65	267.858
868.88	265.446	434.91	268.664
772.25	266.170		
	T = 312.750 K		
959.38	268.804	534.77	271.688
858.54	269.494	441.68	272.312
729.55	270.371	394.20	272.630
636.23	271.003		
	T = 322.750 K		
929.78	273.533	522.36	276.021
832.63	274.131	412.26	276.687
735.59	274.723	314.03	277.276
624.83	275.397		
	T = 332.750 K		
958.15	277.777	544.84	280.054
857.33	278.334	520.66	280.185
755.50	278.895	415.50	280.761
664.72	279.393	316.28	281.299

[a]Uncertainty of temperature: $U(T)$ = 5 mK; uncertainty of pressure: $U(p)$ = 200 Pa; and relative standard uncertainty of speed of sound $U_r(u)$ = 0.02 % (level of confidence = 0.95).

Wagner[68] are shown in Figure 2. The present data measured with a cylindrical resonator show positive relative deviations of between (0.0039 and 0.026) % from the equation of state.[68] Estrada-Alexanders and Trusler[44] measured the speed of sound for carbon dioxide from (220 to 450) K and pressures up to 14 MPa using a spherical resonator. Most of the data from Estrada-Alexanders and Trusler[44] are higher than the results calculated by the equation of state[68] with the highest deviation of 0.088 % at 450 K and 14.2 MPa, with only several data points showing negative deviations with the lowest deviation of −0.018 % at 275 K and 420.54 kPa. Estrada-Alexanders and Hurly[69] measured the speed of sound using an acoustic Greenspan viscometer with a relative standard uncertainty of 0.01 % from (220 to 370) K and pressures up to 3.1 MPa. The speed-of-sound data of Estrada-Alexanders and Hurly[69] show positive deviations from the equation of state[68] except for the data measured at 220 K and 479.78 kPa. The relative deviations of the present data are slightly higher than those of Estrada-Alexanders and Trusler[44] but lower than those of Estrada-Alexanders and Hurly.[69] The relative deviations of the present data and the data of Estrada-Alexanders and Hurly[69] increase as the pressure increases. The equation of state[68] was developed without using the speed-of-sound data measured by acoustic methods. Thus, the measured speed-of-sound data in this work and the results from Estrada-Alexanders and Trusler[44] and Estrada-Alexanders and Hurly[69] can be used to improve the equation of state for carbon dioxide in the future.

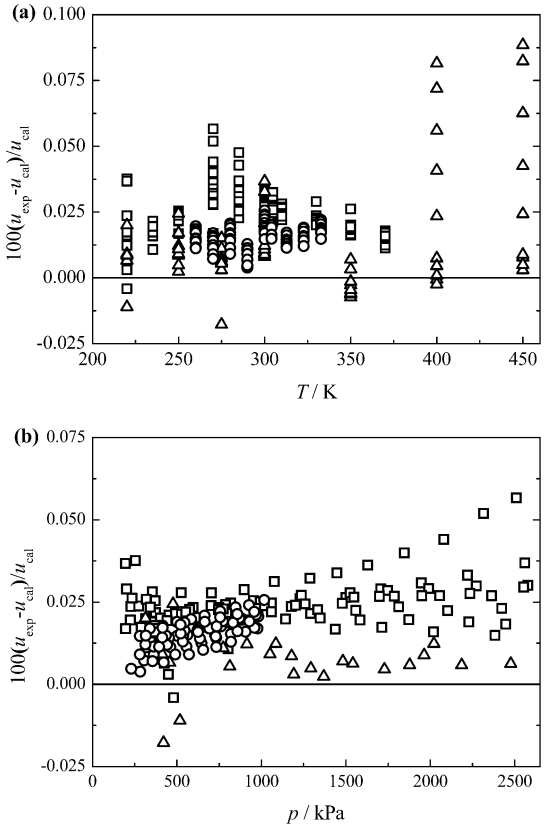

Figure 2. Relative deviations of the measured speed-of-sound data for gaseous carbon dioxide from the equation of state developed by Span and Wagner[68] (a) $100(u_{exp} - u_{cal})/u_{cal}$ vs T and (b) $100(u_{exp} - u_{cal})/u_{cal}$ vs p: ○, this work; △, Estrada-Alexanders and Trusler;[44] □, Estrada-Alexanders and Hurly.[69]

The measured speed-of-sound data for gaseous propene along eight isotherms from (260 to 330) K with pressures up to 1 MPa that are less than 80 % of the saturation pressure to prevent precondensation are shown in Figure 3. Table 3 lists the speed-of-sound data for propene at each temperature and pressure. The relative standard uncertainty of the speed of sound was estimated to be less than 0.02 % including the

dx.doi.org/10.1021/je500424b | J. Chem. Eng. Data 2014, 59, 2788−2798

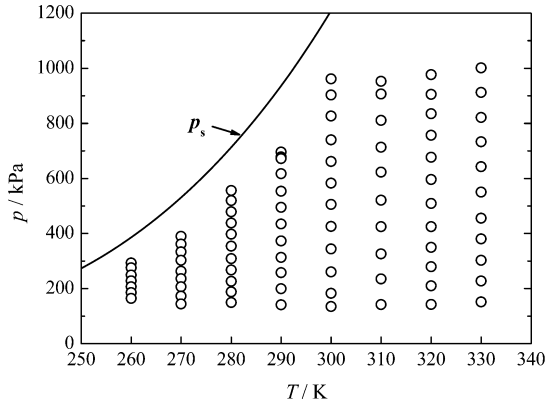

Figure 3. Distributions of the measured speed-of-sound data for gaseous propene in the $p-T$ diagram.

temperature measurement uncertainty, the pressure measurement uncertainty, the frequency measurement uncertainty, and the sample purity uncertainty.

Angus et al.,[70] Overhoff,[71] and Lemmon et al.[72] developed equations of state for propene in 1980, 2006, and 2013, respectively. Lemmon et al.[72] used the speed of sound in the liquid and supercritical regions measured by Meier and Kabelac[73] to optimize the equation of state. Therefore, the equation of state of Lemmon et al.[72] was selected as the reference for the present speed-of-sound data. The deviations of the measured speed-of-sound data relative to the calculated results from the equation of state[72] for propene are shown in Figure 4. The measured speed-of-sound data have negative deviations from the equation of state[72] at 260 K and 270 K with the largest deviation of −0.039 % at 260 K and 293.1 kPa, while most of the speed-of-sound data show positive deviations from (280 to 330) K with the largest deviation of about 0.05 % at 320 K and 976.9 kPa. The measured speed-of-sound data at lower pressures agree well with the equation of state[72] from (280 to 330) K. The deviations of the present speed-of-sound data from the equation of state[72] increase with increasing pressure as shown in Figure 4b. Meier and Kabelac[73] measured the speed of sound in the liquid and supercritical regions with an uncertainty of 0.015 % using a double-path-length pulse-echo technique. However, the speed-of-sound data from Meier and Kabelac[73] show deviations of between −0.08 % and 0.12 % from the equation of state.[72]

3.2. Ideal Gas Heat Capacity at Constant Pressure. The measured speed-of-sound data were fitted to the acoustic virial expansion for each isotherm:

$$u^2 = \frac{\gamma_0 RT}{M}\left(1 + \frac{\beta_a}{RT}p + \frac{\gamma_a}{RT}p^2 + \frac{\delta_a}{RT}p^3\right) \quad (5)$$

where γ_0 is the ratio of the constant pressure to constant volume ideal gas heat capacities, (c_p^0/c_v^0), R = 8.314472 J·mol^{-1}·K^{-1} is the universal gas constant, M is the molar mass, and β_a, γ_a, and δ_a are the second, third, and fourth acoustic virial coefficients.

The ideal gas heat capacity ratio, γ_0, was determined by extrapolating eq 5 to zero pressure for each isotherm. Then, the ideal gas heat capacity at constant pressure was calculated as

$$\frac{c_p^0}{R} = \frac{\gamma_0}{\gamma_0 - 1} \quad (6)$$

Table 3. Measured Speed of Sound Data for Gaseous Propene[a]

p/kPa	u/m·s^{-1}	p/kPa	u/m·s^{-1}
	T = 260.000 K		
293.11	232.483	206.56	236.232
275.35	233.169	185.32	237.147
248.96	234.363	164.45	238.028
227.97	235.295		
	T = 270.000 K		
389.41	233.762	263.03	239.000
361.31	234.964	236.28	240.061
333.53	236.130	206.19	241.233
302.89	237.393	173.01	242.506
262.89	239.005	144.04	243.598
	T = 280.000 K		
556.25	232.732	354.13	240.694
519.72	234.242	308.73	242.368
478.89	235.889	267.79	243.845
438.30	237.487	226.29	245.315
438.33	237.486	188.35	246.636
397.57	239.056	149.29	247.972
	T = 290.000 K		
695.54	233.484	434.96	243.061
677.98	234.169	372.80	245.178
672.07	234.402	313.39	247.152
616.94	236.509	257.68	248.961
553.22	238.872	199.13	250.820
495.22	240.952	141.01	252.628
	T = 300.000 K		
960.98	230.066	505.72	246.037
903.31	232.289	425.25	248.556
826.40	235.145	344.40	251.013
740.35	238.219	260.81	253.485
661.10	240.945	182.30	255.747
582.66	243.559	134.71	257.089
	T = 310.000 K		
952.69	237.373	520.89	250.748
906.76	238.902	424.89	253.463
810.73	242.008	325.91	256.182
713.38	245.043	235.24	258.606
623.06	247.765	142.07	261.046
	T = 320.000 K		
976.94	243.091	509.07	256.044
905.02	245.205	425.07	258.192
834.83	247.220	349.85	260.081
756.59	249.417	279.66	261.8119
677.09	251.597	210.07	263.494
596.12	253.766	142.67	265.102
	T = 330.000 K		
1001.35	248.498	455.62	262.043
912.04	250.844	380.89	263.766
821.61	253.162	302.35	265.548
732.74	255.390	227.66	267.217
642.65	257.599	151.93	268.885
550.82	259.806		

[a]Uncertainty of temperature: $U(T)$ = 5 mK; uncertainty of pressure: $U(p)$ = 200 Pa and relative standard uncertainty of speed of sound $U_r(u)$ = 0.02 % (level of confidence = 0.95).

The determined c_p^0/R values were correlated using the temperature-dependent polynomial function:

dx.doi.org/10.1021/je500424b | J. Chem. Eng. Data 2014, 59, 2788−2798

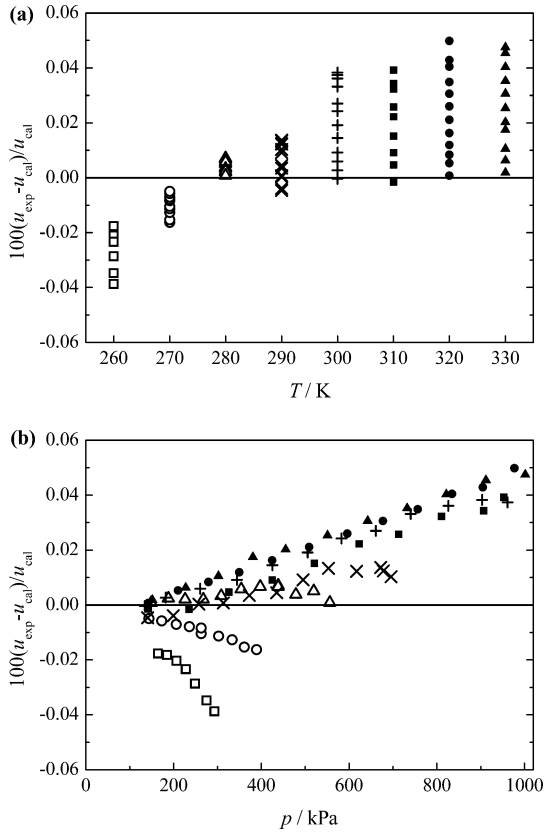

Figure 4. Relative deviations of the measured speed-of-sound data for gaseous propene from the equation of state developed by Lemmon et al.:[72] (a) $100(u_{exp} - u_{cal})/u_{cal}$ vs T and (b) $100(u_{exp} - u_{cal})/u_{cal}$ vs p: □, 260 K; ○, 270 K; △ 280 K; ×, 290 K; +, 300 K; ■, 310 K; ●, 320 K; ▲, 330 K.

$$\frac{c_p^0}{R} = \sum_{i=0}^{2} c_i \left(\frac{T}{T_c}\right)^i \quad (7)$$

where c_i are correlation coefficients, and T_c is the critical temperature with T_c = 304.128 K for carbon dioxide and T_c = 364.211 K for propene.

The determined values of (c_p^0/R) and the second acoustic virial coefficients resulting from four-term fits to the speed-of-sound data are listed in Table 4 for carbon dioxide. The determined correlation coefficients, c_i, in eq 7 for carbon dioxide are listed in Table 5. Equation 7 provides a good description of the determined ideal gas heat capacities at constant pressure in this work with a maximum difference of 0.0009 R.

Table 4. Ideal Gas Heat Capacities and the Second Acoustic Virial Coefficients for Carbon Dioxide Derived from the Measured Speed of Sound Data[a]

T/K	c_p^0/R	β_a/(cm^3·mol^{-1})
260	4.249	−191.1
270	4.309	−174.8
280	4.366	−160.2
290	4.422	−148.5
300	4.475	−135.9
304.09	4.497	−132.4
312.75	4.545	−123.3
322.75	4.598	−113.4
332.75	4.650	−103.3

[a]Relative uncertainty of the ideal gas heat capacity: $U(c_p^0)$ = 0.1 %; and uncertainty of the second acoustic virial coefficient $U(\beta_a)$ = 0.5 cm^3·mol^{-1} (level of confidence = 0.95).

Table 5. Correlation Coefficients, c_i, in eq 7 for Carbon Dioxide and Propene

i	carbon dioxide	propene
0	2.41378	3.34900
1	2.51955	3.88059
2	−0.434803	1.81541

Figure 5 shows the relative deviations of the ideal gas heat capacities for carbon dioxide from the equation of state of Span

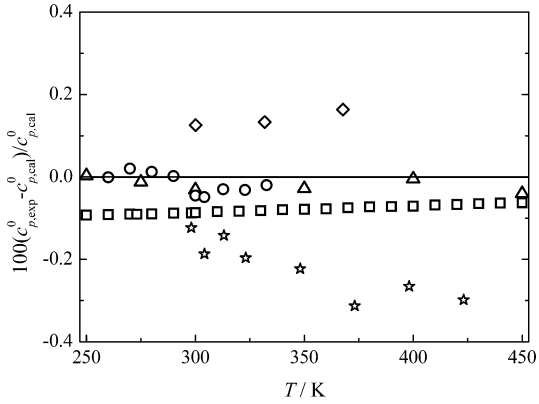

Figure 5. Relative deviations of c_p^0 for carbon dioxide from the equation of state:[68] ○, this work; △, Estrada-Alexanders;[74] □, Baehr et al.;[75] ☆, de Groot and Michels;[76] ◇, Kistiakowsky and Rice.[77]

and Wagner.[68] The ideal gas heat capacities determined in this work agree within 0.05 % with the equation of state of Span and Wagner.[68] The results in this work also match well with the ideal gas heat capacities from the speed-of-sound data measured with a spherical resonator.[74] The ideal gas heat capacities from Baehr et al.[75] show deviations of between −0.06 % and −0.09 % from the equation of state.[68] The results from de Groot and Michels[76] have negative deviations larger than −0.1 % from the results calculated by the equation of state[68] which increase with increasing temperature. The ideal gas heat capacities from Kistiakowsky and Rice[77] are higher than the results from the equation of state[68] by about 0.13 %.

The ideal gas heat capacities and the second acoustic virial coefficient for propene were determined by fitting the measured speed-of-sound data with eq 5. The values of (c_p^0/R) and β_a resulting from four-term fits to the acoustic data are listed in Table 6. The determined correlation coefficients, c_i, in eq 7 for propene are also listed in Table 5. The ideal gas heat capacities at constant pressure calculated by eq 7 agree well with the data listed in Table 6 with a maximum difference of 0.0035 R.

The relative deviations of the ideal gas heat capacities for propene relative to the calculated results from the equation of state[72] are shown in Figure 6. The determined c_p^0 in this work agrees within 0.095 % of the results calculated using the equation of state.[72] The present determined c_p^0 is also in good agreement with the results of Chao and Zwolinski[78] based on a statistical thermodynamic method. The measurements from

dx.doi.org/10.1021/je500424b | J. Chem. Eng. Data 2014, 59, 2788−2798

Table 6. Ideal Gas Heat Capacities and the Second Acoustic Virial Coefficients for Propene Derived from the Measured Speed of Sound Data[a]

T/K	c_p^0/R	β_a/(cm^3·mol^{-1})
260	7.044	−692
270	7.225	−638
280	7.404	−594
290	7.592	−557
300	7.776	−520
310	7.965	−489
320	8.164	−456
330	8.354	−429

[a]Relative uncertainty of the ideal gas heat capacity: $U(c_p^0)$ = 0.1 %; and uncertainty of the second acoustic virial coefficient $U(\beta_a)$ = 3 cm^3·mol^{-1} (level of confidence = 0.95).

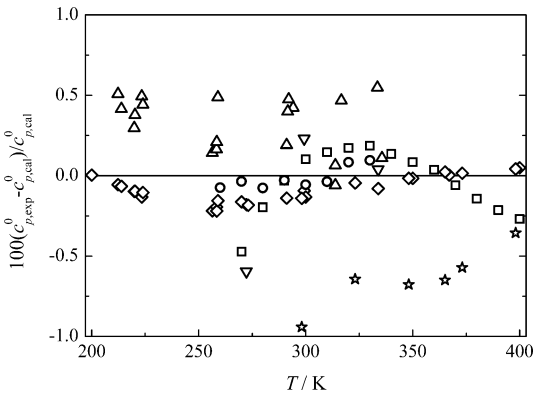

Figure 6. Relative deviations of c_p^0 for propene from the equation of state developed by Lemmon et al.:[72] ○, this work; ◇, Chao and Zwolinski;[78] □, Telfair;[79] △, Kistiakowsky et al.;[80] ▽, Kistiakowsky and Rice;[81] ☆, Bier et al.[82]

Telfair[79] agree well with the equation of state[72] within 0.47 % from (270 to 350) K; most of the results from Kistiakowsky et al.,[80] Kistiakowsky and Rice,[81] and Bier et al.[82] show deviations larger than 0.2 % from the equation of state.[72]

3.3. Second Virial Coefficient. The second acoustic virial coefficient, $\beta_a(T)$, is related to the second virial coefficient, B, as

$$\beta_a = 2B + 2(\gamma_0 - 1)T\frac{dB}{dT} + \frac{(\gamma_0 - 1)^2}{\gamma_0}T^2\frac{d^2B}{dT^2} \quad (8)$$

The acoustic virial coefficients were obtained by fitting the measured speed-of-sound data at each isotherm as listed in Table 4 for carbon dioxide and in Table 6 for propene. The square-well intermolecular potential model[28,30,34,41,45,46,83] can be used to calculate the virial coefficient, $B(T)$, using eq 8. The square-well intermolecular potential model is given by

$$U(r) = \begin{cases} \infty, & r < \sigma \\ -\varepsilon, & \sigma \le r \le R_{rel}\sigma \\ 0, & r > R_{rel}\sigma \end{cases} \quad (9)$$

where r is the distance between molecular centers, ε is the well depth, σ is the hard core radius, and R_{rel} is the ratio of the width of the well to the width of the hard core.

The relationship between $B(T)$ and the square-well parameters is

$$B(T) = b_0[1 - (R_{rel}^3 - 1)\Delta] \quad (10)$$

where $b_0 = 2\pi N_A\sigma^3/3$ is the molar volume of the hard core, N_A is Avogadro's number, $\Delta = \exp[\varepsilon/k_BT] - 1$ and k_B is the Boltzmann constant.

The square-well parameters for carbon dioxide obtained by fitting the second acoustic virial coefficients are listed in Table 7. Thus, the correlation for the second virial coefficient of carbon dioxide is

$$B(T) = 131.531 - 83.1734\cdot\exp(333.752/T) \quad (11)$$

Table 7. Square-Well Parameters for Carbon Dioxide and Propene Obtained by Fitting the Second Acoustic Virial Coefficients

substance	σ/Å	R_{rel}	(ε/k_B)/K
carbon dioxide	3.37199	1.39590	333.752
propene	4.56518	1.50305	289.051

The uncertainty of the calculated second virial coefficient from eq 11 for carbon dioxide was estimated to be 0.8 cm^3·mol^{-1} from (260 to 333) K in view of the assessment of the uncertainty of the second acoustic virial coefficients, the fit quality, and the agreement with literature data. The deviations of the calculated second virial coefficients from this work using eq 11 and other published data for carbon dioxide are shown in Figure 7 relative to the Span and Wagner equation.[68] The second virial coefficients calculated using eq 11 agree with the Span and Wagner equation[68] within ± 0.5 cm^3·mol^{-1} and with the Dymond et al.[84] equation within ± 0.4 cm^3·mol^{-1} from (220 to 320) K and within ± 0.3 cm^3·mol^{-1} from (320 to 480) K. The calculated results from the Estrada-Alexanders and Trusler[44] equation developed from acoustic measurements using a spherical resonator show negative deviations compared to eq 11, the Span and Wagner equation,[68] and the Dymond et al. equation[84] from (250 to 370) K. The calculated results of eq 11 are in good agreement with the experimental results. Holste et al.,[85] Patel et al.,[86] Glowka,[87] Ohgaki et al.,[88] and Feng et al.[89] determined the second virial coefficients for carbon dioxide using the Burnett or Burnett-isochoric methods. The results of Holste et al.,[85] differ from eq 11 by less than 0.3 cm^3·mol^{-1}. The second virial coefficients from Patel et al.[86] agree well with eq 11 within 0.05 cm^3·mol^{-1} at 423.15 K and 448.15 K and show the largest deviation of 0.7 cm^3·mol^{-1} at 373.15 K, while the results from Holste et al.,[85] Glowka,[87] and Waxman et al.[90] match well with eq 11 within 0.3 cm^3·mol^{-1} at 373.15 K. The differences between the present result and the data reported by Glowka[87] are less than 0.2 cm^3·mol^{-1}. The second virial coefficient at 423.15 K determined by Ohgaki et al.[88] agrees with eq 11 within 0.2 cm^3·mol^{-1}, but the data at 473.15 K show a positive deviation of 0.8 cm^3·mol^{-1}. The data reported by Feng et al.[89] differs from eq 11 by only 0.09 cm^3·mol^{-1}. The differences between the results of Duschek et al.[91] and eq 11 are less than 0.5 cm^3·mol^{-1}. The second virial coefficients determined by Jaeschke[92] from refractive index measurements differ from eq 11 by 0.2 cm^3·mol^{-1} from (273.15 to 333.15) K. The second virial coefficients of Mantillla et al.[93] from $p-\rho-T$ measurements with a high-pressure single-sinker magnetic suspension densimeter have positive deviations from eq 11 and the equation of state.[68] The results of Michels and Michels[94] show the largest deviation of −1.7 cm^3·mol^{-1} from eq 11 and of −1.5 cm^3·mol^{-1} from the equation of state[68] at 373 K. The second virial coefficients of Estrada-Alexanders et al.[95] using the speed-of-sound data of Estrada-Alexanders and

dx.doi.org/10.1021/je500424b | J. Chem. Eng. Data 2014, 59, 2788−2798

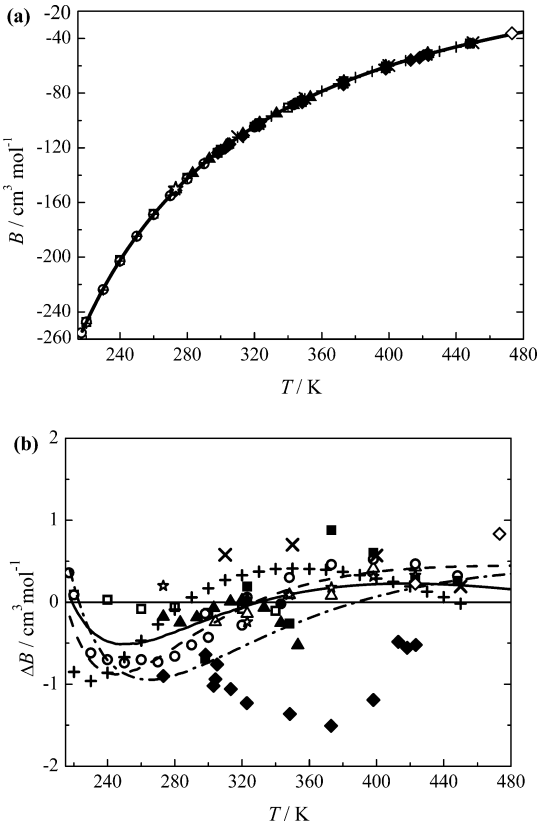

Figure 7. (a) Distributions of the second virial coefficients for carbon dioxide and (b) deviations of the second virial coefficients for carbon dioxide from the equation of state developed by Span and Wagner:[68] —, eq 11; —•—, Estrada-Alexanders and Trusler;[44] ---, Dymond et al.;[84] ○, Holste et al.;[85] ■, Patel et al.;[86] △, Glowka;[87] ◇, Ohgaki et al.;[88] ●, Feng et al.;[89] ☆, Waxman et al.;[90] □, Duschek et al.;[91] ▲, Jaeschke;[92] ×, Mantilla et al.;[93] ♦, Michels and Michels;[94] +, Estrada-Alexanders et al.[95]

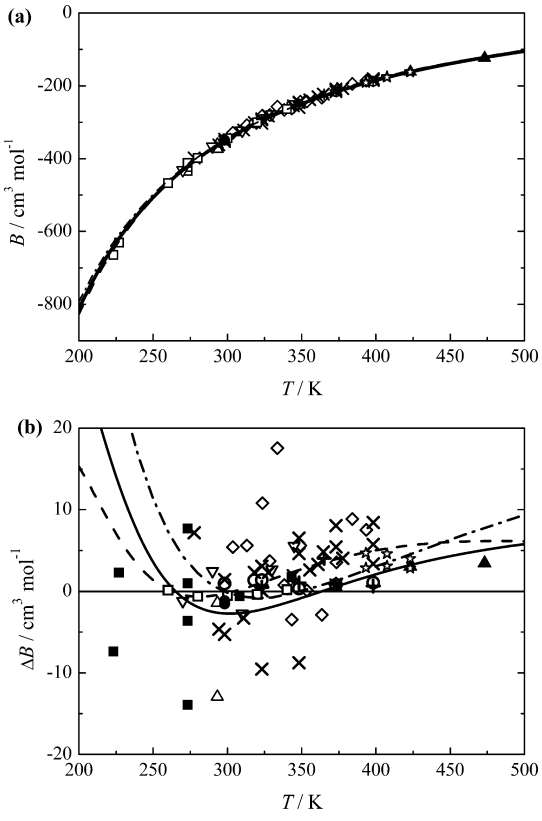

Figure 8. (a) Distributions of the second virial coefficients for propene and (b) deviations of the second virial coefficients for propene from the equation of state developed by Lemmon et al.:[72] —, eq 12; ---, Dymond et al.;[84] —•—, Zarkova and Hohm;[96] +, Bier et al.;[82] ▲, Ohgaki et al.;[88] ☆, Warowny and Stecki;[97] ●, Ohgaki et al.;[98] □, Glos et al.;[99] ○, Michels et al.;[100] ▽, Møllerup;[101] ■, Roper;[102] ◇, McGlashan and Wormald;[103] ×, Pompe and Spurling;[104] △, Lopatinskii et al.[105]

Trusler[44] and of Estrada-Alexanders and Hurly[69] show positive deviations from eq 11 and the experimental results of Feng et al.,[89] Duschek et al.,[91] and Jaeschke[92] from (280 to 380) K.

The square-well parameters for propene obtained by fitting the second acoustic virial coefficients are also listed in Table 7. The second virial coefficient correlation for propene is

$$B(T) = 407.474 - 287.473 \cdot \exp(289.051/T) \qquad (12)$$

The uncertainty of the second virial coefficient from eq 12 for propene was estimated to be within 5 $cm^3 \cdot mol^{-1}$ from (260 to 330) K. The deviations of the calculated second virial coefficients from eq 12 and other published data for propene relative to the equation of state developed by Lemmon et al.[72] are shown in Figure 8. The second virial coefficients calculated using eq 12 agree with the equation of state[72] within ± 5 $cm^3 \cdot mol^{-1}$ and the equation for propene from Dymond et al.[84] within ± 3.5 $cm^3 \cdot mol^{-1}$ from (250 to 470) K. The results of Zarkova and Hohm[96] calculated using a (*n*, 6) Lennard-Jones temperature-dependent potential show positive deviations compared to eq 12, but the deviations are less than 3 $cm^3 \cdot mol^{-1}$ from (300 to 480) K. The results from eq 12, Dymond et al.[84] and Zarkova and Hohm[96] are higher than the results from the equation of state[72] for low temperatures with differences increasing as the temperature decreases. The second virial coefficients from eq 12 are in good agreement with the experimental results. Ohgaki et al.,[88] Warowny and Stecki,[97] and Ohgaki et al.,[98] determined the second virial coefficients for propene using the Burnett method. These three data sets differ from eq 12 by less than 3 $cm^3 \cdot mol^{-1}$, but the results from Ohgaki et al.[88] and Warowny and Stecki[97] differ from the equation of state[72] by more than 3 $cm^3 \cdot mol^{-1}$. The second virial coefficients of propene measured by Glos et al.[99] using an accurate two-sinker densimeter agree with the equation of state[72] within 0.6 $cm^3 \cdot mol^{-1}$ and with eq 12 within 1.2 $cm^3 \cdot mol^{-1}$ because these data sets were the main sets used to develop the reference equation of state.[72] The second virial coefficients from Bier et al.,[82] Michels et al,.[100] and Møllerup[101] also match well with eq 12. The data reported by Roper,[102] McGlashan and Wormal,[103] Pompe and Spurling[104] and Lopatinskii et al.[105] show somewhat larger differences than the other data.

■ CONCLUSIONS

The speed of sound was measured in gaseous carbon dioxide from (260 to 332.75) K and in gaseous propene from (260 to 330) K with pressures up to 1000 kPa using a cylindrical resonator. The thermal and viscous boundary disturbances, the gas fill duct disturbance, the shell motion disturbance, and the vibrational relaxation disturbance were corrected in the frequency measurements. The relative standard uncertainty in the speed of sound measurements was estimated to be less than 0.02 %. The present speed-of-sound data for gaseous carbon

dx.doi.org/10.1021/je500424b | J. Chem. Eng. Data 2014, 59, 2788−2798

dioxide agrees within the uncertainties with the results from Estrada-Alexanders and Trusler.[44] No previous speed of sound for gaseous propene has been published; thus, the current data will be useful for improving the equation of state for propene.

The ideal-gas heat capacities at constant pressure for carbon dioxide and propene were deduced from the measured speed of sound with an uncertainty of 0.1 %. The present ideal gas heat capacities are in good agreement with high-precision experimental data. The present ideal gas heat capacities for carbon dioxide agree within 0.05 % with the Span and Wagner equation,[68] while the results for propene agree within 0.095 % with the Lemmon et al. equation.[72]

The density second virial coefficients, $B(T)$, were then obtained from the speed-of-sound data and the square-well intermolecular model. The second virial coefficients from the present correlations agree within the uncertainties of the high-precision experimental data or calculated data from EoS.

AUTHOR INFORMATION

Corresponding Author

*Tel.: +86 10 62796318. Fax: +86 10 62770209. E-mail: yyduan@tsinghua.edu.cn.

Funding

This work was supported by the National Natural Science Foundation of China (Grant Nos. 51076074, 51236004 and 51106143).

Notes

The authors declare no competing financial interest.

ACKNOWLEDGMENTS

All equation of state calculations were performed with the NIST Standard Reference Database 23 REFPROP version 9.0.

REFERENCES

(1) Tao, Y. B.; He, Y. L.; Tao, W. Q. Exergetic analysis of transcritical CO_2 residential air conditioning system based on experimental data. *Appl. Energy* **2010**, *87*, 3065−3072.

(2) Yang, J. L.; Ma, Y. T.; Li, M. X.; Hua, J. Modeling and simulating the transcritical CO_2 heat pump system. *Energy* **2010**, *35*, 4812−4818.

(3) Bhatkar, V. W.; Kriplani, V. M.; Awari, G. K. Alternative refrigerants in vapor compression refrigeration cycle for sustainable environment: A review of recent research. *Int. J. Environ. Sci. Technol.* **2013**, *10*, 871−880.

(4) Yang, Z.; Wu, X. Retrofits and options for the alternatives to HCFC-22. *Energy* **2013**, *59*, 1−21.

(5) Chang, Y. S.; Kim, M. S.; Ro, S. T. Performance and heat transfer characteristics of hydrocarbon refrigerants in a heat pump system. *Int. J. Refrig.* **2000**, *23*, 232−242.

(6) Chaichana, C.; Lu, A.; Charters, W. W. S. Natural working fluids for solar boosted heat pumps. *Int. J. Refrig.* **2003**, *26*, 637−643.

(7) Palm, B. Hydrocarbons as refrigerants in small heat pump and refrigeration systems—A review. *Int. J. Refrig.* **2008**, *31*, 552−563.

(8) Mohanraj, M.; Jayaraj, S.; Muraleedharan, C. Environment friendly alternatives to halogenated refrigerants—A review. *Int. J. Greenhouse Gas Control* **2009**, *3*, 108−119.

(9) Park, K. J.; Jung, D. S. Thermodynamic performance of HCFC22 alternative refrigerants for residential air-conditioning application. *Energy Build.* **2007**, *39*, 675−680.

(10) Park, K. J.; Jung, D. S. Thermodynamic performance of R502 alternative refrigerant mixtures for low temperature and transport applications. *Energy Convers. Manage.* **2007**, *48*, 3084−3089.

(11) Saleh, B.; Koglbauer, G.; Wendland, M.; Fischer, J. Working fluids for low-temperature organic Rankine cycles. *Energy* **2007**, *32*, 1210−1221.

(12) Guo, T.; Wang, H. X.; Zhang, S. J. Fluids and parameters optimization for a novel cogeneration system driven by low-temperature geothermal sources. *Energy* **2011**, *36*, 2639−2649.

(13) Lai, N. A.; Wendland, M.; Fischer, J. Working fluids for high-temperature organic Rankine cycles. *Energy* **2011**, *36*, 199−211.

(14) Liu, Q.; Duan, Y. Y.; Yang, Z. Performance analyses of geothermal organic Rankine cycles with selected hydrocarbon working fluids. *Energy* **2013**, *63*, 123−132.

(15) Tchanche, B. F.; Papadakis, G.; Lambrinos, G.; Frangoudakis, A. Fluid selection for a low-temperature solar organic Rankine cycle. *Appl. Therm. Eng.* **2009**, *29*, 2468−2476.

(16) Outcalt, S. L.; Lemmon, E. W. Bubble-point measurements of eight binary mixtures for organic Rankine cycle applications. *J. Chem. Eng. Data* **2013**, *58*, 1853−1860.

(17) Liu, Q.; Duan, Y. Y.; Yang, Z. Effect of condensation temperature glide on the performance of organic Rankine cycles with zeotropic mixture working fluids. *Appl. Energy* **2014**, *115*, 394−404.

(18) Baik, Y. J.; Kim, M.; Chang, K. C.; Kim, S. J. Power-based performance comparison between carbon dioxide and R125 transcritical cycles for a low-grade heat source. *Appl. Energy* **2011**, *88*, 892−898.

(19) Zhang, S. J.; Wang, H. X.; Guo, T. Performance comparison and parametric optimization of subcritical organic Rankine cycle (ORC) and transcritical power cycle system for low-temperature geothermal power generation. *Appl. Energy* **2011**, *88*, 2740−2754.

(20) Guo, T.; Wang, H. X.; Zhang, S. J. Comparative analysis of natural and conventional working fluids for use in transcritical Rankine cycle using low-temperature geothermal source. *Int. J. Energy Res.* **2011**, *35*, 530−544.

(21) Vetter, C.; Wiemer, H. J.; Kuhn, D. Comparison of sub- and supercritical organic Rankine cycles for power generation from low-temperature/low-enthalpy geothermal wells, considering specific net power output and efficiency. *Appl. Therm. Eng.* **2013**, *51*, 871−879.

(22) Walraven, D.; Laenen, B.; D'haeseleer, W. Comparison of thermodynamic cycles for power production from low-temperature geothermal heat sources. *Energy Convers. Manage.* **2013**, *66*, 220−233.

(23) Li, H.; Bu, X.; Wang, L.; Long, Z.; Lian, Y. Hydrocarbon working fluids for a Rankine cycle powered vapor compression refrigeration system using low-grade thermal energy. *Energy Build.* **2013**, *65*, 167−172.

(24) Wu, J. T.; Zhou, Y. An equation of state for fluoroethane (R161). *Int. J. Thermophys.* **2012**, *33*, 220−234.

(25) Ewing, M. B.; Goodwin, A. R. H.; McGlashan, M. L.; Trusler, J. P. M. Thermophysical properties of alkanes from speeds of sound determined using a spherical resonator. 1. Apparatus, acoustic model, and results for dimethylpropane. *J. Chem. Thermodyn.* **1987**, *19*, 721−739.

(26) Trusler, J. P. M. *Physical Acoustics and Metrology of Fluids*; Adam Hilger: Bristol, England, 1991.

(27) Kano, Y.; Kayukawa, Y.; Fujii, K.; Sato, H. Ideal gas heat capacity derived from speed of sound measurements in the gaseous phase for trans-1,3,3,3-tetrafluoropropene. *J. Chem. Eng. Data* **2013**, *58*, 2966−2969.

(28) Gillis, K. A.; Moldover, M. R. Practical determination of gas densities from the speed of sound using square-well potentials. *Int. J. Thermophys.* **1996**, *17*, 1305−1324.

(29) Trusler, J. P. M.; Wakeham, W. A.; Zarari, M. P. Second and third interaction virial coefficients of the (methane plus propane) system determined from the speed of sound. *Int. J. Thermophys.* **1996**, *17*, 35−42.

(30) Hurly, J. J.; Schmidt, J. W.; Gillis, K. A. Virial equation of state and ideal-gas heat capacities of pentafluoro-dimethyl ether. *Int. J. Thermophys.* **1997**, *18*, 137−159.

(31) Trusler, J. P. M.; Wakeham, W. A.; Zarari, M. P. Model intermolecular potentials and virial coefficients determined from the speed of sound. *Mol. Phys.* **1997**, *90*, 695−703.

(32) Liu, Q.; Feng, X. J.; Duan, Y. Y. Determination of the second virial coefficient for working fluid using a cylindrical resonator. *Chem. Ind. Eng. Soc. China J.* **2013**, *64*, 2711−2717 (in Chinese).
(33) Estrada-Alexanders, A. F.; Trusler, J. P. M. The speed of sound and derived thermodynamic properties of ethane at temperatures between 220 and 450 K and pressures up to 10.5 MPa. *J. Chem. Thermodyn.* **1997**, *29*, 991−1015.
(34) Goodwin, A. R. H.; Marsh, K. N.; Wakeham, W. A. *Measurement of the Thermodynamic Properties of Single Phases*; Elsevier: Amsterdam, Netherlands, 2003.
(35) Trusler, J. P. M.; Zarari, M. The speed of sound and derived thermodynamic properties of methane at temperatures between 275 and 375 K and pressures up to 10 MPa. *J. Chem. Thermodyn.* **1992**, *24*, 973−991.
(36) Dayton, T. C.; Beyerlein, S. W.; Goodwin, A. R. H. Determination of densities and heat capacities from speed of sound measurements for 1,1,1,2-tetrafluoroethane. *J. Chem. Thermodyn.* **1999**, *31*, 847−868.
(37) Duan, Y. Y.; Sun, L. Q.; Shi, L.; Zhu, M. S.; Han, L. Z. Speed of sound and ideal-gas heat capacity at constant pressure of gaseous trifluorodomethane (CF_3I). *Fluid Phase Equilib.* **1997**, *137*, 121−131.
(38) Sun, L. Q.; Duan, Y. Y.; Shi, L.; Zhu, M. S.; Han, L. Z. Speed of sound and ideal-gas heat capacity at constant pressure of gaseous difluoromethane. *J. Chem. Eng. Data* **1997**, *42*, 795−799.
(39) Zhang, C.; Duan, Y. Y.; Shi, L.; Zhu, M. S.; Han, L. Z. Speed of sound, ideal-gas heat capacity at constant pressure, and second virial coefficients of HFC-227ea. *Fluid Phase Equilib.* **2001**, *178*, 73−85.
(40) Ewing, M. B.; Goodwin, A. R. H. Thermophysical properties of alkanes from speeds of sound determined using a spherical resonator. 4. 2-Methylpropane at temperatures in the range 251 to 320 K and pressures in the range 5 to 114 kPa. *J. Chem. Thermodyn.* **1991**, *23*, 1107−1120.
(41) Gillis, K. A. Thermodynamic properties of 2 gaseous halogenated ethers from speed of sound measurements difluoromethoxy-difluoromethane and 2-difluoromethoxy-1,1,1-trifluoroethane. *Int. J. Thermophys.* **1994**, *15*, 821−847.
(42) Gillis, K. A. Thermodynamic properties of seven gaseous halogenated hydrocarbons from acoustic measurements: $CHClFCF_3$, CHF_2CF_3, CF_3CH_3, CHF_2CH_3, $CF_3CHFCHF_2$, $CF_3CH_2CF_3$, and $CHF_2CF_2CH_2F$. *Int. J. Thermophys.* **1997**, *18*, 73−135.
(43) Hozumi, T.; Sato, H.; Watanabe, K. Speed-of-sound measurements in gaseous binary refrigerant mixtures of difluoromethane (R32) + 1,1,1,2-tetrafluoroethance (R134a). *J. Chem. Eng. Data* **1997**, *42*, 541−547.
(44) Estrada-Alexanders, A. F.; Trusler, J. P. M. Speed of sound in carbon dioxide at temperatures between (220 and 450) K and pressures up to 14 MPa. *J. Chem. Thermodyn.* **1998**, *30*, 1589−1601.
(45) Goodwin, A. R. H.; Moldover, M. R. Thermophysical properties of gaseous refrigerants from speed of sound measurements. 1. Apparatus, model, and results for 1,1,1,2-tetrafluoroethane R134a. *J. Chem. Phys.* **1990**, *93*, 2741−2753.
(46) Hurly, J. J. Thermophysical properties of chlorine from speed-of-sound measurements. *Int. J. Thermophys.* **2002**, *23*, 455−475.
(47) Benedetto, G.; Gavioso, R. M.; Spagnolo, R.; Grigiante, M.; Scalabrin, G. Vapor-phase Helmholtz equation for HFC-227ea from speed-of-sound measurements. *Int. J. Thermophys.* **2001**, *22*, 1073−1088.
(48) He, M. G.; Liu, Z. G.; Yin, J. M. Measurement of speed of sound with a spherical resonator: HCFC-22, HFC-152a, HFC-143a, and propane. *Int. J. Thermophys.* **2002**, *23*, 1599−1615.
(49) Moldover, M. R.; Trusler, J. P. M.; Edwards, T. J. Measurement of the universal gas constant *R* using a spherical acoustic resonator. *J. Res. Natl. Bur. Stand.* **1988**, *93*, 85−144.
(50) Gavioso, R. M.; Benedetto, G.; Giuliano Albo, P. A.; Merlone, A.; Balsamo, A.; D'Errico, G. E.; Spagnolo, R. Progress towards an acoustic measurement of the molar gas constant at INRIM. *Int. J. Thermophys.* **2007**, *28*, 1775−1788.
(51) Gavioso, R. M.; Benedetto, G.; Giuliano Albo, P. A.; Merlone, A.; Guianvarc'h, C.; Moro, F.; Cuccaro, F. A determination of the Boltzmann constant from speed of sound measurements in helium at a single thermodynamic state. *Metrologia* **2010**, *47*, 387−409.
(52) Sutton, G.; Underwood, R.; Pitre, L.; de Podesta, M.; Valkiers, S. Acoustic resonator experiments at the triple point of water: First results for the Boltzmann constant and remaining challenges. *Int. J. Thermophys.* **2010**, *31*, 1310−1346.
(53) Zhang, J. T.; Lin, H.; Feng, X. J.; Sun, J. P.; Gillis, K. A.; Moldover, M. R.; Duan, Y. Y. Progress toward redetermining the Boltzmann constant with a fixed-path-length cylindrical resonator. *Int. J. Thermophys.* **2011**, *32*, 1297−1329.
(54) Lin, H.; Feng, X. J.; Gillis, K. A.; Moldover, M. R.; Zhang, J. T.; Sun, J. P.; Duan, Y. Y. Improved determination of the Boltzmann constant using a single, fixed-length cylindrical cavity. *Metrologia* **2013**, *50*, 417−432.
(55) Ewing, M. B.; Trusler, J. P. M. Primary acoustic thermometry between T = 90 K and T = 300 K. *J. Chem. Thermodyn.* **2000**, *32*, 1229−1255.
(56) Benedetto, G.; Gavioso, R. M.; Spagnolo, R.; Marcarino, P.; Merlone, A. Acoustic measurements of the thermodynamic temperature between the triple point of mercury and 380 K. *Metrologia* **2004**, *41*, 74−98.
(57) Pitre, L.; Moldover, M. R.; Tew, W. L. Acoustic thermometry: New results from 273 to 77 K and progress towards 4 K. *Metrologia* **2006**, *43*, 142−162.
(58) Ripple, D. C.; Strouse, G. F.; Moldover, M. R. Acoustic thermometry results from 271 to 552 K. *Int. J. Thermophys.* **2007**, *28*, 1789−1799.
(59) Feng, X. J.; Gillis, K. A.; Moldover, M. R.; Mehl, J. B. Microwave-cavity measurements for gas thermometry up to the copper point. *Metrologia* **2013**, *50*, 219−226.
(60) Moldover, M. R.; Gavioso, R. M.; Mehl, J. B.; Piter, L.; de Podesta, M.; Zhang, J. T. Acoustic gas thermometry. *Metrologia* **2014**, *51*, R1−R19.
(61) Zhang, J. T.; Lin, H.; Sun, J. P.; Feng, X. J.; Gillis, K. A.; Moldover, M. R. Cylindrical acoustic resonator for the re-determining of the Boltzmann constant. *Int. J. Thermophys.* **2010**, *31*, 1273−1293.
(62) Gillis, K. A.; Lin, H.; Moldover, M. R. Perturbations from ducts on the modes of acoustic thermometers. *J. Res. Natl. Inst. Stand. Technol.* **2009**, *114*, 263−285.
(63) Lin, H.; Gillis, K. A.; Zhang, J. T. Characterization of piezoelectric ceramic transducer for accurate speed-of-sound measurement. *Int. J. Thermophys.* **2010**, *31*, 1234−1247.
(64) Feng, X. J.; Lin, H.; Liu, Q.; Zhou, M. X.; Duan, Y. Y. Fundamental theory and apparatus for speed of sound measurement system using cylindrical resonator. *J. Eng. Thermophys.* **2011**, *32*, 725−728 (in Chinese).
(65) Tegeler, Ch.; Span, R.; Wagner, W. A new equation of state for argon covering the fluid region for temperatures from the melting line to 700 K at pressures up to 1000 MPa. *J. Phys. Chem. Ref. Data* **1999**, *28*, 779−850.
(66) Lemmon, E. W.; Jacobsen, R. T. Viscosity and thermal conductivity equations for nitrogen, oxygen, argon, and air. *Int. J. Thermophys.* **2004**, *25*, 21−69.
(67) Mehl, J. B.; Moldover, M. R. Pre-condensation phenomena in acoustic measurements. *J. Chem. Phys.* **1982**, *77*, 455−465.
(68) Span, R.; Wagner, W. A new equation of state for carbon dioxide covering the fluid region from the triple-point temperature to 1100 K at pressures up to 800 MPa. *J. Phys. Chem. Ref. Data* **1996**, *25*, 1509−1596.
(69) Estrada-Alexanders, A. F.; Hurly, J. J. Kinematic viscosity and speed of sound in gaseous CO, CO_2, SiF_4, SF_6, C_4F_8, and NH_3 from 220 to 375 K and pressures up to 3.4 MPa. *J. Chem. Thermodyn.* **2008**, *40*, 193−202.
(70) Angus, S.; Armstrong, B.; de Reuck, K. M. *International Tables of the Fluid State-7 Propylene (Propene)*; Pergamon: Oxford, U.K., 1980.
(71) Overhoff, U. *Development of a new equation of state for the fluid region of propene for temperatures from the melting line to 575 K with pressures to 1000 MPa as well as software for the computation of*

thermodynamic properties of fluids. Ph.D. Dissertation, Ruhr Universität, Bochum, Germany, 2006.
(72) Lemmon, E. W.; Overhoff, U.; McLinden, M. O.; Wagner, W. A reference equation of state for the thermodynamic properties of propene for temperatures from the melting line to 575 K and pressures up to 1000 MPa. 2013. Unpublished work.
(73) Meier, K.; Kabelac, S. Measurements of the speed of sound in propene in the liquid and supercritical regions. *J. Chem. Eng. Data* **2013**, *58*, 1621−1628.
(74) Estrada-Alexanders, A. F. *Thermodynamic properties of gases from measurements of the speed of sound*. Ph.D. Dissertation; University of London, London, 1996.
(75) Baehr, H. D.; Hartmann, H.; Pohl, H. C.; Schomäcker, H. *Thermodynamische funktionen idealer gase für themperaturen bis 6000 K*; Springer-Verlag: Berlin, 1968.
(76) de Groot, S. R.; Michels, A. The Joule-Thomson effect and the specific heat at constant pressure of carbon dioxide. *Physica* **1948**, *14*, 218−222.
(77) Kistiakowsky, G. B.; Rice, W. W. Gaseous heat capacities I. The method and the heat capacities of C_2H_6 and C_2D_6. *J. Chem. Phys.* **1939**, *7*, 281−288.
(78) Chao, J.; Zwolinski, B. J. Ideal gas thermodynamic properties of ethylene and propylene. *J. Phys. Chem. Ref. Data* **1975**, *4*, 251−261.
(79) Telfair, D. Supersonic measurement of the heat capacity of propylene. *J. Chem. Phys.* **1942**, *10*, 167−171.
(80) Kistiakowsky, G. B.; Lacher, J. R.; Ransom, W. W. The low temperature gaseous heat capacities of certain C3 hydrocarbons. *J. Chem. Phys.* **1940**, *8*, 970−977.
(81) Kistiakowsky, G. B.; Rice, W. W. Gaseous heat capacities. II. *J. Chem. Phys.* **1940**, *8*, 610−618.
(82) Bier, K.; Ernst, G.; Kunze, J.; Maurer, G. Thermodynamic properties of propylene from calorimetric measurements. *J. Chem. Thermodyn.* **1974**, *6*, 1039−1052.
(83) Estela-Uribe, J. F. An improved Helmholtz energy model for non-polar fluids and their mixtures. Part 2: Application to mixtures of non-polar fluids. *Fluid Phase Equilib.* **2013**, *354*, 326−343.
(84) Dymond, J. H.; Mash, K. N.; Wilhoit, R. C. *Virial coefficients of pure gases and mixtures*, Vol. *21*; Springer: New York, 2002.
(85) Holste, J. C.; Hall, K. R.; Eubank, P. T.; Esper, G.; Watson, M. Q.; Warowny, W.; Bailey, D. M.; Young, J. G.; Bellomy, M. T. Experimental (p, V_m, T) for pure CO_2 between 220 and 450 K. *J. Chem. Thermodyn.* **1987**, *19*, 1233−1250.
(86) Patel, M. R.; Joffrion, L. L.; Eubank, P. T. A simple procedure for estimating virial coefficients from Burnett *pvT* data. *AIChE J.* **1988**, *34*, 1229−1232.
(87) Glowka, S. Determination of volumetric properties of ammonia between 298 and 473 K and carbon dioxide between 304 and 423 K using the Burnett method. *Polym. J. Chem.* **1990**, *64*, 699−709.
(88) Ohgaki, K.; Sakai, N.; Kano, Y.; Katayama, T. Experimental study of second virial coefficients for carbon dioxide, methane, ethylene, and propylene at 423.15 and 473.15 K. *J. Chem. Eng. Jpn.* **1984**, *17*, 545−547.
(89) Feng, X. J.; Liu, Q.; Zhou, M. X.; Duan, Y. Y. Gaseous *pvTx* properties of mixtures of carbon dioxide and propane with the Burnett isochoric method. *J. Chem. Eng. Data* **2010**, *55*, 3400−3409.
(90) Waxman, M.; Davis, H. A.; Hastings, J. R. A new determination of the second virial coefficient of carbon dioxide at temperatures between 0 °C and 150 °C and an evaluation of its reliability. *Proc. 6th Symp. Thermophys. Prop.* **1973**, 245−255.
(91) Duschek, W.; Kleinrahm, R.; Wagner, W. Measurement and correlation of the (pressure, density, temperature) relation of carbon-dioxide. 1. The homogeneous gas and liquid regions in the temperature-range from 217 to 340 K at pressures up to 9 MPa. *J. Chem. Thermodyn.* **1990**, *22*, 827−840.
(92) Jaeschke, M. Determination of the interaction second virial coefficients for the carbon dioxide-ethane system from refractive index measurements. *Int. J. Thermophys.* **1987**, *8*, 81−95.
(93) Mantilla, I. D.; Cristancho, D. E.; Ejaz, S.; Hall, K. R.; Atilhan, M.; Iglesias-Silva, G. A. p-ρ-T data for carbon dioxide from (310 to 450) K up to 160 MPa. *J. Chem. Eng. Data* **2010**, *55*, 4611−4613.
(94) Michels, A.; Michels, C. Isotherms of CO_2 between 0°C and 150°C and pressures from 16 to 250 atm. *Proc. R. Soc. London, Ser. A* **1935**, *153*, 201−214.
(95) Estrada-Alexanders, A. F.; Guzmán, O.; Pérez-Vidal, B. High-precision virial coefficients of argon and carbon dioxide from integration of speed of sound data in the pressure-temperature domain. *Mol. Phys.* **2012**, *110*, 1349−1358.
(96) Zarkova, L.; Hohm, U. Effective (n − 6) Lennard-Jones potentials with temperature-dependent parameters introduced for accurate calculation of equilibrium and transport properties of ethene, propene, butene, and cyclopropane. *J. Chem. Eng. Data* **2009**, *54*, 1648−1655.
(97) Warowny, W.; Stecki, J. Compressibility, second and third virial coefficients and interaction second virial coefficients of mixtures of propane-helium and propene-helium. *J. Chem. Eng. Data* **1978**, *23*, 212−216.
(98) Ohgaki, K.; Mizuhaya, T.; Katayama, T. The interaction second virial coefficients for seven binary systems containing carbon dioxide, methane, ethylene, ethane, and propylene at 25°C. *J. Chem. Eng. Jpn.* **1981**, *14*, 71−72.
(99) Glos, S.; Kleinrahm, R.; Wagner, W. Measurement of the (p,ρ,T) relation of propane, propylene, *n*-butane, and isobutene in the temperature range from (95 to 340) K at pressures up to 12 MPa using an accurate two-sinker densimeter. *J. Chem. Thermodyn.* **2004**, *36*, 1037−1059.
(100) Michels, A.; Wassenaar, T.; Louwerse, P.; Lunbeck, R. J.; Wolkers, G. J. Isotherms and thermodynamical functions of propene at temperatures between 25°C and 150°C and at densities up to 340 amagat (pressures up to 2800 atm). *Physica* **1953**, *19*, 287−297.
(101) M?llerup, J. Measurement of the volumetric properties of methane and ethene at 310 K at pressures to 70 MPa and of propene from 270 to 345 K at pressures to 3 MPa by the Burnett method. *J. Chem. Thermodyn.* **1985**, *17*, 489−499.
(102) Roper, E. E. Gas imperfection. I. Experimental determination of second virial coefficients for seven unsaturated aliphatic hydrocarbons. *J. Phys. Chem.* **1940**, *44*, 835−847.
(103) McGlashan, M. L.; Wormald, C. J. Second virial coefficients of some alk-l-enes, and of a mixture of propene + hept-l-ene. *Trans. Faraday Soc.* **1964**, *60*, 646−652.
(104) Pompe, A.; Spurling, T. H. *Virial Coefficients for Gaseous Hydrocarbons*; POMP-A 74-1012, Technical Paper No. 1; CSIRO: Melbourne Australia, 1974.
(105) Lopatinskii, E. S.; Rozhnov, M. S.; Zhdanov, V. I.; Parnovskii, S. L.; Kudrya, Y. N. Second virial coefficient of gas mixtures of hydrocarbons, carbon dioxide and hydrogen with nitrogen and argon. *Zh. Fiz. Khim.* **1991**, *65*, 2060−2065.